

SDSS J122958.84+000138.0: A Compact, Optically red galaxy ^{*}

Sanjaya Paudel^{1†}, Thorsten Lisker², Avon P. Huxor² and Chang H. Ree¹

¹*Korea Astronomy and Space Science Institute, Daejeon 305-348, Republic of Korea*

²*Astronomisches Rechen-Institut, Zentrum für Astronomie der Universität Heidelberg, Mönchhofstraße 12-14, 69120 Heidelberg, Germany*

14 November 2016

ABSTRACT

We report a new compact galaxy, SDSS J122958.84+000138.0 (SDSS J1229+0001), which has unique morphological and stellar population properties that are rare in observations of the nearby universe. SDSS J1229+0001 has an r -band absolute magnitude (M_r) and half-light radius (R_h) of -17.75 mag and 520 pc, respectively. Located in a fairly low density environment, morphologically it is akin to a typical early-type galaxy as it has a smooth appearance and red colour. But, interestingly, it possesses centrally concentrated star forming activity with a significant amount of dust. We present an analysis of structural and stellar population properties using archival images and VLT/FORS2 spectroscopy. Analysis of UKIDSS H-band image shows that the observed light distribution is better fitted with two components Sérsic function with inner and outer component effective radii 190 and 330 pc, respectively. Whereas, overall half-light radius measured in H-band is much smaller compared to optical, i.e 290 pc. We prepared a Spectral Energy Distribution (SED) from optical to FIR and interpret it to derive star-formation rate, dust mass and stellar mass. We find that the SDSS J1229+0001 has dust mass $M_{dust} = 5.1 \times 10^5 M_\odot$ with a dust to stellar mass ratio $\log(M_{dust}/M_*) = -3.5$. While the observed stellar population properties are – to some extent – similar to that of a typical S0 galaxy, a unified view from stellar population and structural properties may suggests that SDSS J1229+0001 is a *smoking gun* example of a compact early-type galaxy in formation.

Key words: galaxies: dwarf - galaxies: formation - galaxies: evolution - galaxies: elliptical - galaxies: individual SDSS J122958.84+000138.0 - galaxies: star formation

1 INTRODUCTION

Correlations and anti-correlations between galaxy parameters, known as scaling relations, have been used to understand the underlying physical principles of galaxy formation. Of particular interest is the size-luminosity relation, which has received considerable attention in recent studies of galaxy of formation and evolution (e.g. Kormendy (1985); Janz & Lisker (2008)). However, observational data exhibit both a large scatter and a significant number of outliers (Graham & Guzmán 2003; Kormendy et al. 2009; Chen et al. 2010; Misgeld & Hilker 2011). There exist a compact class of galaxies, compact ellipticals (cEs), which do not follow the Log(size)-magnitude relation and becomes an outlier

(Chilingarian et al. 2009; Trujillo et al. 2009; Paudel et al. 2014). They are compact, high surface brightness, metal-rich and possess a large velocity dispersion compared to the majority of similar mass galaxies, i.e. early-type dwarfs (dEs). So, their origin and evolution are expected to be different from that of dEs, the majority population. Number of studies discussing the origins of these compact galaxies have reached to the conclusions that are contradictory to each other (Trujillo et al. 2007; Paudel et al. 2014; Graham et al. 2015; Stringer et al. 2015).

With advent of large scale surveys and high-resolution imaging instruments, an increasing number of cEs have been reported (Chilingarian et al. 2009; Chilingarian & Zolotukhin 2015). They are found in a range of environments: from the densest galaxy cluster centre, to the field (Mieske et al. 2005; Huxor et al. 2011, 2013; Paudel et al. 2014; Price et al. 2009). However, an overwhelm majority of known cEs are located in dense environments, particularly around massive galaxies. Therefore, several studies propose an origin

^{*} Based on observations collected at the European Organisation for Astronomical Research in the Southern Hemisphere, Chile (programme 087.B-0841(A))

[†] E-mail: sjy@kasi.re.kr

via tidal stripping, where strong tidal forces from a nearby massive host galaxy strips off the entire outer-disk component during the interaction and the remnant inner bulge becomes a naked compact galaxy (Bekki et al. 2001; Choi et al. 2002). Huxor et al. (2011) discovered two cEs, each near a massive host and with clear tidal debris, confirming this picture. Other hand, cEs are also found in isolation or less dense environments (Huxor et al. 2013; Paudel et al. 2014; Chilingarian & Zolotukhin 2015) and in the absence of such strong tidal force, it is therefore naively expected that not all cEs might have formed via tidal stripping. Chilingarian & Zolotukhin (2015) has, however, suggested that all such isolated cEs can be explained as runaway systems, ejected from a galaxy group or cluster by three-body encounters.

Here, we present a new compact galaxy, SDSS J1229+0001, which, from its morphology, seems to be an early-type galaxy, visually selected to create an early-type galaxy sample from the Sloan Digital Sky Survey (SDSS) colour images. The presence of strong emission in H α in optical spectrum, however, indicates a burst of ongoing star-formation similar to a typical Blue Compact Dwarf (BCD) (Hopkins et al. 2002).

2 DATA ANALYSIS

We perform a detailed analysis of imaging and spectroscopic data to characterise the stellar population and structural properties of this galaxy. The multi-wavelength study covering the range from optical to far-infrared data, and based on various archival images, allows us to make an accurate estimation of stellar mass, dust mass and internal extinction. We obtained long-slit spectroscopic observation using ESO-VLT that supplements these data. Comparing the derived stellar population and structural properties with those of a well-studied sample of galaxies, we try to explore its possible evolution and origin which may provide some important clue in understanding of the formation and evolution of compact galaxies in the nearby Universe.

2.1 Environment and Identification

We first conducted a systematic search of low-mass early-type galaxies in the field environment of the local volume ($z < 0.01$) to catalogue and study the physical and stellar population parameters of those galaxies located in the isolation. For this purpose we derived the distance to the nearest massive galaxies in terms of sky projected separation and relative velocities (see Paudel et al. 2014) and selected the early-type morphology by visual inspection of the SDSS DR7 colour images (Abazajian et al. 2009).

SDSS J122958.84+000138.0 (hereafter SDSS J1229+0001) is located in a relatively isolated environment south of the Virgo cluster, at an angular separation of ~ 8 degree from M49. The nearest bright galaxy is NGC 4517 is at $\sim 45'$ (440 kpc) east although the relative radial velocity between the two is 1285 km s^{-1} . But the closest galaxy in term of sky-projected distance and relative radial velocity is SDSS J123002.09-002438.0; located at ~ 190 kpc south

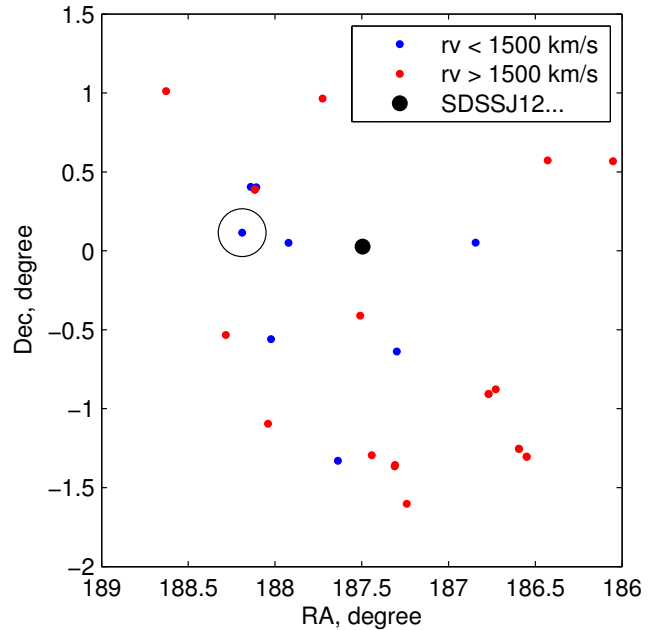


Figure 1. Distribution of the line of sight radial velocities over a range of 3000 km/s of galaxies around SDSS J1229+0001. The red and blue dots represents galaxies which radial velocity larger and smaller than 1500 km s^{-1} , respectively. A large solid black dot represents SDSS J1229+0001 and the black circle is the position of NGC 4517, where the two have line of sight radial velocities of 2413 km s^{-1} and 1128 km s^{-1} , respectively.

and with a relative radial velocity¹ 98 km s^{-1} but have a luminosity of $M_r = -14.71$ mag.

In Figure 1, we show distribution of galaxy around SDSS J1229+0001 within a radius of $100'$ and redshift range of $z = 0.001$ to 0.01 . The galaxy sample is obtained from a NED query. The sample is divided into two redshift bins, i.e. $z < 0.005$ and $z > 0.005$, represented by blue and red points respectively. SDSS J1229+0001 is represented by large solid dot and a big circle represents NGC 4517, having line of sight radial velocities of 2413 km s^{-1} and 1128 km s^{-1} respectively. According to a catalogue of nearby groups (Makarov & Karachentsev 2011), SDSS J1229+0001 is not assigned to be a member of any nearby group. Interestingly, NGC 4517 is also considered an isolated disk galaxy in Doyle et al. (2005) and galaxy population in this region of sky seems to be relatively sparse. Within this the sky coverage shown in the Figure 1, no rich galaxy group has been found.

2.2 Imaging

At first, we used the SDSS image to perform image analysis. We particularly made use of r -band image, which has a higher signal to noise ratio than the other bands. The archival images of SDSS-III has better sky-background subtraction than the previous data releases. We, further, subtracted the sky-background using the procedure in Paudel

¹ Redshift measured by 2DF survey (Colless et al. 2001) which report the line of sight radial velocities of SDSS J1229+0001 and it's companion 2408.1 and 2310.0 km/s, respectively.



Figure 2. Optical view of the SDSS J1229+0001 with a field of view of $1' \times 1'$.

Top: We show colour-image cutout from the SDSS

Bottom: We show major axis profile measured from IRAF/ellipse. In second panel we show $g - i$ colour gradient (without corrections for either internal and external extinction). Where the vertical dash line represent the r -band PSF.

et al. (2014) where we selected the sky-background counts from randomly selected sky-regions around the galaxy to derive the median background.

The IRAF task *ellipse* was used to extract the galaxy's major-axis light profile. We used similar procedure as in Paudel et al. (2014) to prepare input image and to run ellipse task. In Figure 2, we show $g - r - i$ combined colour image cut-out in top panel which is we obtained from the SDSS sky-server. At first glance, it gives a visual impression of S0 galaxy with a prominent dust lane at the centre,

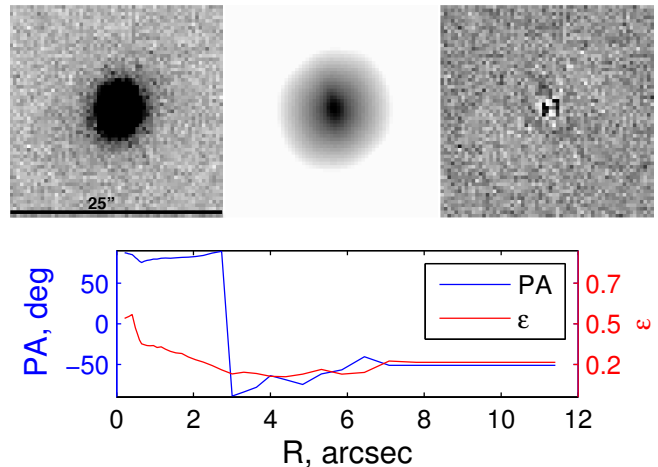


Figure 3. Modelling of galaxy light distribution with GALFIT. We show the H-band image, the model and the residual in left, middle and right panel, respectively. We show variation of ellipticity (red) and PA (blue) along the major axis in bottom panel.

perpendicular to the major axis of the galaxy. We show the major axis light profile and $g - i$ colour profile in bottom panel of Figure 2. The colour gradient was derived from the azimuthally-averaged light profiles in the g and i -band. Since a difference in PSF can produce an artificial colour gradient at the centre of galaxies, we matched the PSFs of these images by degrading the better image. We find that PSFs in g and i -band are $1.04''$ and $0.92''$, respectively.

Since the central part of the galaxy heavily obscured by dust, to model the galaxy light distribution and derive structural parameter we used UKIDSS² H-band image expecting that the H-band image is less affected by dust extinction. We retrieved stacked H-band image from WSA - WFCAM Science Archive³ which has spatial sampling of $0.4''$ and the spatial resolution is comparable to the SDSS with a seeing of $0.84''$. We used GALFIT to perform two dimensional modeling. The required PSF image is also provided during GALFIT run. We find that the two dimensional light distribution is better modeled with two component Sérsic function. We show result of GALFIT run in top panel of Figure 3. Where we show, from left to right, the H-band image, the model and the model subtracted residual, respectively. We also run IRAF *ellipse* task in H-band image to derive variation of ellipse parameter along the major axis that we show in lower panel of Figure 3. The average ellipticity of the galaxy is 0.21.

Non parametric approach has been used to calculate photometric parameters, i.e half-light radius and total luminosity. Where a two Petrosian radius aperture has been used to summed up the total flux. We follow a similar procedure as described in Janz & Lisker (2008); Paudel et al. (2014) where we used major axis Petrosian radius. The major axis half-light radius is circularized by multiplying a factor of $(1 - \epsilon)^{0.5}$ where ϵ is an average ellipticity of the galaxy. The mean surface brightness within the half-light radius is calculated by using the equation $\langle \mu \rangle = m + 2.5 \log[2\pi R_h^2]$, where R_h

² <http://www.ukidss.org>

³ <http://wsa.roe.ac.uk>

Table 1. Multi-wavelength data

Filters	Lambda_eff μ	Flux jy
SDSS u'	0.35	$2.4\text{E-}4 \pm 0.5\text{E-}5$
SDSS g'	0.46	$9.42\text{E-}4 \pm 0.5\text{E-}5$
SDSS r'	0.61	$2.07\text{E-}3 \pm 0.5\text{E-}5$
SDSS i'	0.74	$3.36\text{E-}3 \pm 0.5\text{E-}5$
SDSS z'	0.89	$3.90\text{E-}3 \pm 1\text{E-}5$
UKIDSS J	1.25	$8.44\text{E-}3 \pm 1\text{E-}5$
UKIDSS H	1.65	$11.35\text{E-}3 \pm 1\text{E-}5$
UKIDSS K	2.20	$9.68\text{E-}3 \pm 1\text{E-}5$
IRAC1	3.56	$4.83\text{E-}3 \pm 4\text{E-}5$
IRAC2	4.51	$3.54\text{E-}3 \pm 3\text{E-}5$
IRAC3	5.76	$13.36\text{E-}3 \pm 1\text{E-}4$
IRAC4	8.00	$39.18\text{E-}3 \pm 1\text{E-}4$
WISE3	12.0	$24.20\text{E-}3 \pm 1\text{E-}3$
WISE4	22.0	$62.11\text{E-}3 \pm 1\text{E-}3$
MIPS24	24.0	$0.06 \pm 1\text{E-}3$
IRS60	60	$0.81 \pm 2\text{E-}3$
IRS100	100	$1.08 \pm 5\text{E-}2$
AKARI140	140	$0.38 \pm 1\text{E-}1$
AKARI160	160	$0.20 \pm 1\text{E-}1$

is half-light radius in arcsec. The results are presented in Table 3, where the magnitudes are corrected for both Galactic and internal extinction. The value of Galactic extinction is obtained from NED and the internal extinction due to dust is derived from the SED fitting (see below).

In this work, adopted a cosmology with $H_0 = 71$ and $\Omega_m = 0.3$. Using the Hubble flow we obtained a distance to the galaxy is 34.0 Mpc and spatial scale $0.163 \text{ kpc arcsec}^{-1}$.

Fortunately, we find that substantial multi-wavelength data are available in various archives, allowing us to create a Spectral Energy Distribution (SED) from the optical to the far infra-red (FIR). The SDSS provides optical $-u, g, r, i$ and z -bands images. We obtained corrected UKIDSS J, H and K band magnitudes from RCSED⁴. We use the IRSA⁵ archive to obtain NIR images (Spitzer observations) and measure the total flux using aperture photometry. The CDS⁶ catalogue server is queried to acquire the MIR and FIR fluxes. Where 24μ , 12μ and 22μ fluxes were measured in the Spitzer MIPS24, WISE3⁷ and WISE4 imaging bands, respectively. The FIR data points are taken from the Infrared Astronomical Satellite (IRAS) and AKARI⁸ all sky surveys. The measured fluxes in respective wave-bands in Janskys are given in Table 1.

The publicly available code MAGPHYS (da Cunha et al. 2008) was used to analyse the observed SED. The main principle behind it, in brief, is to check the energy balance that are emitted from several different components, i.e. young and old stellar emission, absorption due to dust and re-emission in FIR. First a model SED is created using Bruzual & Charlot (2003) library of templates computing integrated stellar light and superposing an attenuation curve due to dust for a varying set of model parameters such

as SFR, age and metallicity. The dust attenuation curve is derived from a simple analytic model of Charlot & Fall (2000). Finally, applying a χ^2 -minimisation scheme, MAGPHYS tries to find the best fit model template for a particular set of physical parameters. This code does not consider a potential AGN contribution and only star formation processes are involved in building the SEDs. However, we investigate any possibility of AGN presence by looking its position in BPT diagram (Baldwin et al. 1981). We use the emission line flux measured from central spectrum to construct the BPT diagram, and find that SDSS J1229+0001 is unambiguously located in the region of star-forming galaxies.

A comparison between the observed SED and the best fit template is shown in Figure 4, where the red dots represent the observe photometric data points and the black and blue lines are the best fit SEDs for the non-attenuated and dust-attenuated model, respectively. In general, the model SED seems to be able to well characterise the observed data points. A slight deviation, however, is seen in the FIR region that may indicate the necessity of longer wavelength data points, unfortunately not available, to better constrain the physical parameters of the model. In particular, longer wavelength data are crucial in making an accurate estimate of dust temperature.

The resulting physical parameters: total stellar mass, dust mass, extinction and metallicity are reported in last panel of Table 3. We derive the SDSS r -band extinction, A_r , from the flux ratio between the dust-attenuated and non-attenuated model i.e. the black and blue line in Figure 4, respectively.

2.3 Spectroscopy

We obtained long-slit low-resolution spectroscopic data using VLT FORS2 instrument as a part of ongoing campaign to study low-mass early-type galaxies in different environment. The details of long-slit observation and data reduction were presented in Paudel et al. (2014). The total exposure time for this galaxy was 1000 sec. Following the similar procedure of VLT FORS2 data reduction as described in Paudel et al. (2010) we achieve 0.1 mag accuracy around 5000 Å in calibrating the observed flux that we measured from standard deviation of sensitivity function. The orientation and position of the slit over the galaxy is shown in Figure 5, top panel where the slit is aligned along the major-axis of the galaxy.

The one-dimensional spectrum is extracted by summing the flux in a two-dimensional frame along the spatial direction. To extract a galaxy wide spectrum we use an aperture of $\pm 7''$ (solid red line in Figure 5 top panel). In Figure 6, we show the flux-calibrated one-dimensional spectrum, where the Balmer emission lines are prominent.

We measure the emission line fluxes using the IRAF task *splot* fitting a gaussian profile. The ratio between $H\alpha$ and $H\beta$ flux, so called Balmer decrement c , is 7.8. Using a theoretical value of the $c_0 = 2.86$ for a electron temperature 10^4 K and an electron density $n_e = 10^2 \text{ cm}^{-3}$ (Osterbrock 1989) and the Calzetti et al. (2000) extinction law, we derived the extinction coefficient $E(B-V)$ and corresponding r -band extinction A_r .

Oxygen abundances, $12+\log(\text{O}/\text{H})$, were estimated

⁴ <http://rcsed.sai.msu.ru>

⁵ <http://irsa.ipac.caltech.edu>

⁶ <http://cdsarc.u-strasbg.fr>

⁷ <http://wise.ssl.berkeley.edu>

⁸ <http://www.ir.isas.jaxa.jp>

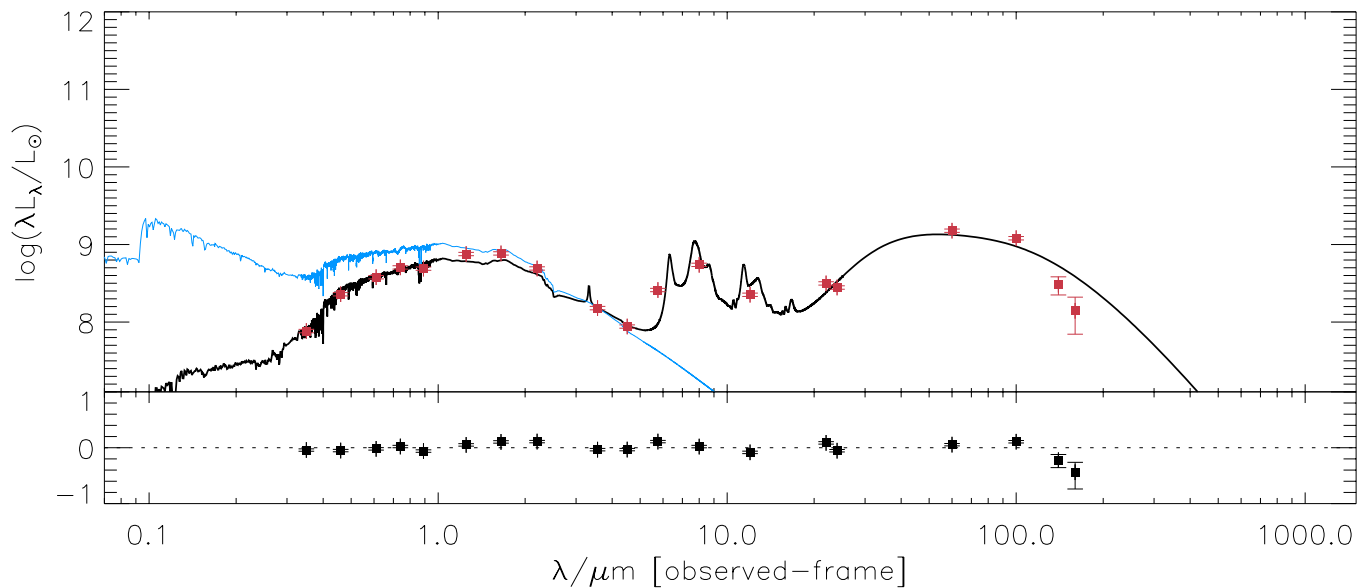


Figure 4. Fitted SED, output from MAGPHYS. The red dots are observed data points of SDSS J1229+0001. The black and blue lines are the best fit SEDs for the non-attenuated and dust-attenuated model, respectively.

with the two methods described by Marino et al. (2013), i.e the so-called N2 and O3N2 methods. The N2 method only considers the line ratio between $H\alpha$ and $[NII]$ while the O3N2 method uses a combination of the line ratios $H\alpha/[NII]$ and $[OIII]/H\beta$. A typical systematic error in these calibrations is 0.2 dex (Denicoló et al. 2002; Marino et al. 2013).

3 RESULTS

Although a typical early-type galaxy as seen in the SDSS colour image, the optical spectroscopy reveals strong Balmer emission (Fig. 6). The star-formation rate derived from $H\alpha$ emission is $\sim 0.25 M_{\odot}/\text{yr}$ and, not surprisingly, as a sign of star-burst activity; the dust lane at centre is clearly visible. Below we present the results from analysis of structural properties and multi-wavelength photometry.

3.1 Image analysis

We find a significant difference in half-light radius measured in optical and H-band imaging. The measured geometric half-light radius of the galaxy from the SDSS r-band is 0.52 kpc whereas that we measured from H-band imaging is significantly less i.e 0.29 kpc. The SDSS z-band the half-light radius is 0.49 kpc. This trend can be well explained by increasing extinction of dust at the centre of the galaxy toward shorter wavelength which significantly reduces the central light concentration.

It was clear from variation of position of PA in inner and outer part that the morphology of the galaxy is not simple. This was further supported by our two-dimensional modelling of light distribution in H-band image using GALFIT. We find that the two component Sérsic function provides better fits than simple Sérsic function. The results are listed in Table 3. The best fit inner and outer component Sérsic indices (n) are 1.4 and 1.2 and effective radii (R_e) 0.19 kpc

Table 3. Derived structural parameter from H-band image. All parameters, other than top three, are the results of GALFIT run. m_H is corrected H-band magnitude listed in RCSED and R_h is half light radius measured from Ptosian method, see text. $\langle \mu_H \rangle$ is an average surface brightness within R_h .

Parameter	value	unit
m_H	14.39	mag
R_h	0.29	kpc
$\langle \mu_H \rangle$	17.53	mag arcsec $^{-2}$
$R_{e,in}$	0.19	kpc
$R_{e,out}$	0.33	kpc
n_{in}	1.4	
n_{out}	1.2	
ϵ_{in}	0.62	
ϵ_{out}	0.08	
PA_{in}	77	degree
PA_{out}	-61	degree

and 0.33 kpc respectively. The inner and outer component has Position Angle 77° and -61° , respectively. We plot ellipticity and position angle profiles along the major axis in the last panel. We find strong change in PA around 2 to 3 arcsec which flips from $\sim 80^\circ$ to $\sim -80^\circ$, Figure 3 bottom panel.

An overall $g-i$ colour index of the galaxy is 1.02 and 1.35 mag, after and before applying the correction for extinction due to dust reddening, respectively. The relation between colour magnitude for various types of low mass galaxies is shown in Figure 7. For this we use tabulated values of r-band absolute magnitude and $g-i$ colour index from Meyer et al. (2014) for BCDs and dEs. For the cEs, we use the photometric parameters from Chilingarian & Mamon (2008); Chilingarian & Bergond (2010). Two green symbols, solid circle and square, represent the extinction corrected and uncorrected $g-i$ colour index of SDSS J1229+0001, respectively. The difference between star-forming galaxies,

Table 2. Global properties: Physical parameter of SDSS J1229+0001. The parameters are grouped according to the results of different analyses. Column 2 – 4 are the results of the SDSS r-band image analysis. The magnitudes are corrected for galactic and internal extinction. R_h is half light radius derived from Petrosian method. Emission line metallicity, $12+\log(\text{O}/\text{H})$, is listed in column 6. The output of the best-fit SED using MAGPHYS are presented in columns 7 – 11.

* Before extinction correction.

	M_r	$g-i$	R_e	z	$12+\log(\text{O}/\text{H})$	$E(\text{B}-\text{V})$	M_*	M_{dust}	A_r	$\log[Z/Z_\odot]$
	mag	mag	kpc		dex	mag	M_\odot	M_\odot	mag	dex
SDSS J122958.84+000138.0	-17.75	1.02 (1.35*)	0.52	0.008	8.5	0.85	1.8E9	5.1E5	0.71	0.008

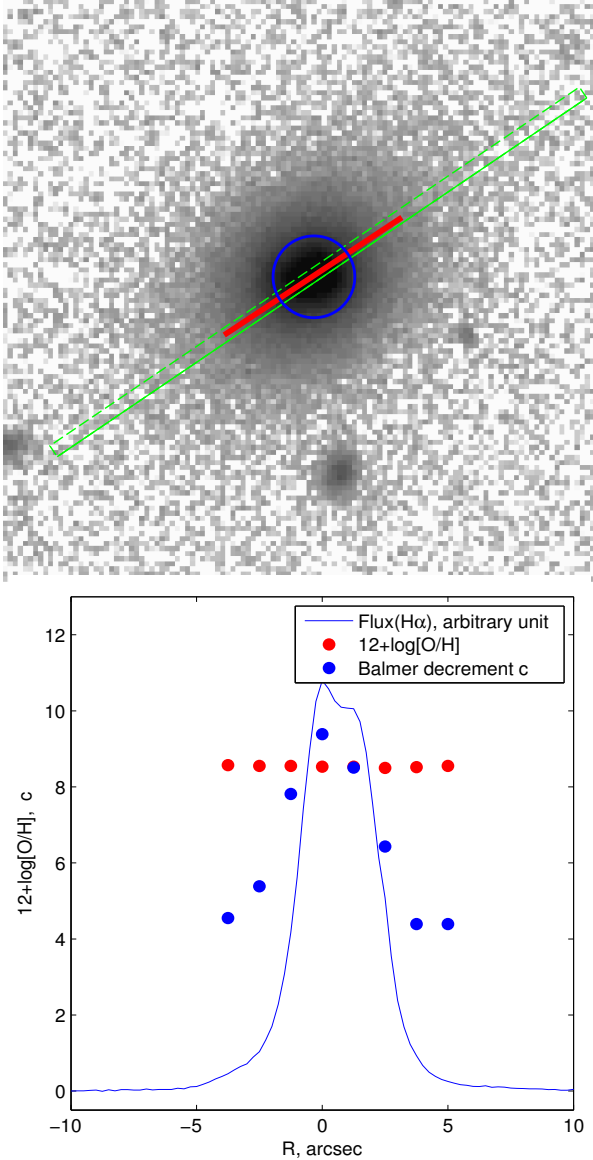


Figure 5. Top: SDSS r-band image where we overlay a one arc-second slit in green colour. The red solid line represents the extension the extension of $\text{H}\alpha$ emission and the radius blue circle is half-radius of galaxy. The field of view is similar to Figure 2. Bottom: $\text{H}\alpha$, gas-phase metallicity and Balmer decrement (c) profile along the major axis.

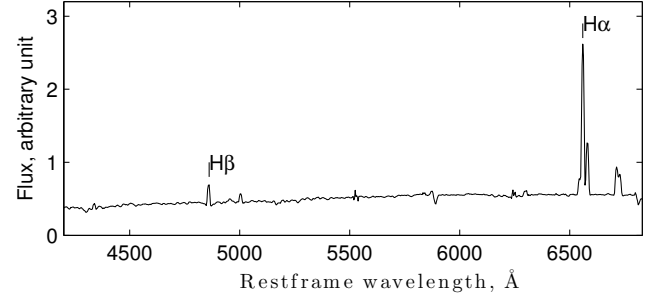


Figure 6. Flux-calibrated VLT2 FORS2 spectrum of SDSS J1229+0001.

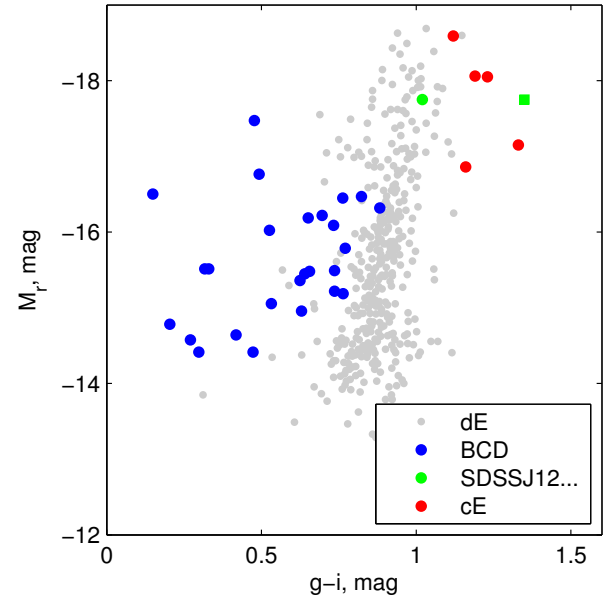


Figure 7. Colour-magnitude relation of dwarf galaxies. BCDs, dEs and cEs are in blue, grey and red, respectively. The green symbols represent SDSS J1229+0001, where the square and circle are for before and after extinction correction, respectively.

BCDs, and others (cEs and dEs) is distinctively clear as previously noted by Meyer et al. (2014), but interestingly SDSS J1229+0001 is consistent with dEs colour being slightly bluer than mean cE colour. Nevertheless, the uncorrected $g-i$ colour of SDSS J1229+0001 is the reddest point in this diagram.

We show the observed $g-i$ colour gradient (uncorrected for extinction) along the major axis in Figure 2, where we

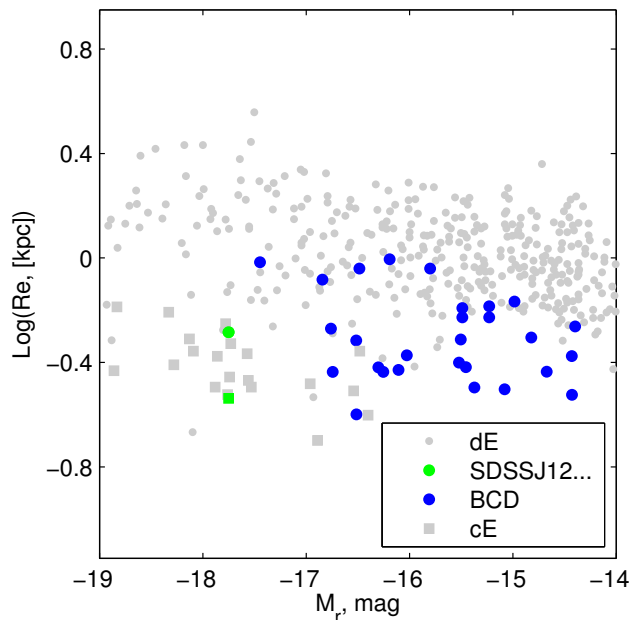


Figure 8. Magnitude-size relation. The green circle and square represent the half-light radius of SDSS J1229+0001 derived from optical and H-band images, respectively. The other of symbols are similar to Figure 7.

can see that steep rise of $g - i$ colour index at the centre with a maximum value 1.4 mag. It becomes nearly constant beyond the $3''$ and have a value similar to that we obtained from the overall colour index after the extinction correction that is obtained from SED fitting.

In Figure 8, we show the relation between sizes and luminosities for the low mass early-type galaxies, using the measurements from Janz & Lisker (2008) for dEs, Es and S0, and Chilingarian et al. for cEs. As previously identified in many studies (Janz & Lisker 2008; Chilingarian et al. 2009; Huxor et al. 2013; Paudel et al. 2014), the distinction between cEs and dEs in this diagram is clearly visible. SDSS J1229+0001 lies in the region of cE being relatively compact compare to similar luminosity dEs or dS0. Note, however, there is also statistical difference in sizes of BCDs and dEs as the latter being more extended system then former, though the scatter in both cases is fairly large.

3.2 Multi-wavelength analysis

The results from the analysis of multi wavelength data, i.e a SED from optical to FIR, are presented in Table 3, fourth panel. The derived total stellar and dust masses are 1.8×10^9 and $5.1 \times 10^5 M_{\odot}$, respectively which gives a value of dust-to-stellar mass ratio, $\log(M_{\text{dust}}/M_{*}) = -3.5$. The metallicity derived from SED fitting agrees well with that from emission lines, being nearly solar at $\log(Z/Z_{\odot}) = 0.008$. However, the internal extinction derived from flux ratio between the Balmer lines is significantly larger than that we have obtained from SED fitting. Comparing the attenuated and non-attenuated best fit SED, we calculate extinction $A_{\lambda} = 2.5 \log(\frac{F_{\lambda}^{\text{non-attenuated}}}{F_{\lambda}^{\text{attenuated}}})$. We obtain $A_r = 0.7$ mag, at wavelength 7500 \AA , and the extinction becomes as high as

Table 4. Star-formation rates

Band	Flux	SFR
	Jy	M_{\odot}/yr
H α	$0.34^{*} \pm 0.005$	0.26
MIPS24 μ	0.06 ± 0.001	0.19
1.4GHz	$(2.9 \pm 0.13) \times 10^{-3}$	0.25
SED fitting	-	0.06

Star-formation rates calculated from different methods.

*The H α flux is obtained by summing up the long-slit spectrum and finally corrected for extinction $A_{\alpha} = 2.3$ mag.

$A_{uv} = 5.9$ mag at Ultra Violet (UV, $\lambda = 1000 \text{ \AA}$) region. We expect this difference in extinction which are derived from different methods because the Balmer decrement only represent the central star-forming region where the presence of dust is pronounce and in the SED fitting we consider overall galaxy photometry.

We derived total star-formation rate from several different diagnostics and respective empirical calibrations. These diagnostic are listed in Table 3.2 where the fluxes are presented in Jansky unit. H α emission line flux is corrected for the internal extinction, but no aperture correction has been made. We use empirical calibrations from Kennicutt (1998); Murphy et al. (2011); Rieke et al. (2009) for the H α , radio and MIPS star-formation diagnostics, respectively. We find that the SFR derived from these three diagnostics are fairly consistent with each other but SED fitting gives a lower value, i.e nearly four time smaller than that from H α or 1.4GHz fluxes. Due to uncertainties in the model, particularly the star-formation history, it is likely that SFR derived from SED fitting without UV photometry is highly uncertain.

3.3 Spectroscopy

We show H α flux profile along the slit in Figure 5, blue line at lower panel. We see nearly two peaks gaussian profile that may hint at some mis-alignment of the elongation of star-forming region at the centre with PA of the galaxy. This is much clearer in the colour image, where the dust lane is almost orthogonal to this PA and probably why the PA profile shows an abrupt change at the centre, see Figure 2. The extension of H α emission along the major axis is greater than $\pm 6''$ from the centre.

The total H α flux measured from integrated spectrum is $2.66 \times 10^{-14} \text{ erg/cm}^2/\text{s}$ ⁹. The ratio between H α and H β flux, Balmer decrement, $c = 7.8$. Which gives $E(B-V) = 1.97 \times \log(c/c_0) = 0.85$ and corresponding r -band extinction $A_r = 3.44$ mag. However note that, we do not use this value of A_r to correct any photometric measurement other than the H α flux to derive star-formation rate, see below.

We obtained $12 + \log(\text{O}/\text{H}) = 8.4(8.5)$ dex from the N2(O3N2). We show metallicity profile along the slit in Figure 5, lower panel red-solid dots. We find a nearly constant gas-phase metallicity along the major axis up to $\sim 2 R_e$

⁹ Without correcting the extinction and aperture effects

4 DISCUSSION AND CONCLUSION

We present a new compact and red looking star-forming galaxy, SDSS J1229+000, which has a half-light radius of 520 pc and relatively steep light profile with Sérsic index $n = 3$. Although, SDSS J1229+0001 has a $g - i$ colour index of 1.02, similar to a typical old “red and dead” early-type galaxy of a similar mass, a strong ongoing star-formation is also observed at the centre, with a $\text{SFR} = \sim 0.25 \text{ M}_{\odot}/\text{yr}$. Nevertheless, an analysis of SED from optical to FIR reveals that a substantial amount of dust is present, i.e. $M_{\text{dust}} = 4.9 \times 10^5 \text{ M}_{\odot}$ with dust-to-stellar mass ratio of $\log(M_{\text{dust}}/M_{*}) = -3.5$.

4.1 Mixed/Intermediate morphology?

Although low mass galaxies are the most common in the universe, their classification scheme is somewhat arbitrary. Particular morphological traits, mainly in the optical bands, are used to define a particular class of galaxies. For example, strongly concentrated star-formation is mostly considered for Blue Compact Dwarf galaxy (BCD) and irregular morphology with low level of star-formation are characteristics of dwarf Irregular galaxies (dIrrs). They are both gas rich and found in relatively low dense environments, such as in the outskirts of galaxy-cluster and in the field. BCDs are, by definition, relatively high surface galaxies compared to dIrrs. Meyer et al. (2014) showed that a number of BCDs (but not all) are structurally similar to compact early-type dwarf galaxies (dEs) and that dIrrs are similar to diffuse dEs.

Among the non star-forming families there exist several types. dEs, dwarf lenticulars (dS0s) and dwarf spheroidals (dSphs) are relatively extended galaxies with low-surface brightnesses. The distinction between them is not straightforward. However, the primary motivation of introducing the dS0 class was the observation of multi-component light profiles in some low mass early-type galaxies in the Virgo cluster (Sandage & Binggeli 1984) – dwarf analogs of the massive S0 galaxies which possess distinct bulge and disk components. Furthermore, Lisker et al. (2007) detailed analysis of sub-structural properties of dEs indeed supports the existence of disk feature in a considerable fraction of dEs. Janz et al. (2014) concluded that the common bulge-plus-disk picture of bright S0s is not applicable, explaining the observed inner and outer components of early-type dwarfs. Moreover, Ryden et al. (1999) earlier noticed no distinction in the structural parameters of these two –dEs and dS0– morphological classes. However, the average dS0 has a brighter surface brightness than the average dE, reflecting the fact that dS0s mostly occur at brighter magnitudes of early-type dwarfs.

At the massive scale, S0 galaxies not only differ from Es in structural parameters but also in stellar population and dust content. More S0 galaxies host ongoing centrally concentrated star formation than Es and also a significantly larger dust mass fraction (Amblard et al. 2014). There are low-mass S0s which have been explicitly classified as S0 at the same mass as dS0s, but which have significantly higher surface brightness, e.g. VCC 1833 or VCC 0140. The dust to stellar mass ratio of $\log(M_{\text{dust}}/M_{*}) = -3.5$ is typical of early-type galaxies at a stellar mass of $\sim 10^9 \text{ M}_{\odot}$ (di Serego Alighieri et al. 2013). SDSS J1229+0001 also exhibits

an unusually high star formation rate and dust mass that compared a typical S0 galaxy. In addition to this, we find that observed light distribution is better described by two component Sérsic function. Overall size, half-light radius, measured in H-band is quite small, i.e. 290 pc. Given that the H-band is more sensitive to the light of old stars than the optical is, this indicates that the galaxy will likely end up in the compact regime once star formation stops.

Compact non-star forming galaxies, somewhat rare in observation, also exist in different names at different stellar masses such as compact ellipticals (cEs) and Ultra Compact Dwarf galaxies (UCDs) possibly form a continuum of a mass range from $\sim 10^6 \text{ M}_{\odot}$ to $\sim 10^9 \text{ M}_{\odot}$ (Norris et al. 2014). Compact ellipticals (cEs) are significantly compact and high surface brightness galaxies compare to low mass S0s and dS0s.

While not denying the possibility of it being a S0 galaxy, our results suggest that SDSS J1229+0001 may be the late stage of a forming compact early-type galaxy. It is worth noting that cEs and S0 morphologies are not mutually exclusive. M32, the type example of an cE, also possesses outer-disk and inner-bulge component which has been a defining character of S0 morphology. Recently, Paudel et al. (2016) reported a compact early-type galaxy with an active nucleus which is structurally similar to a typical S0 galaxies.

4.2 Relative rarity of the object

In this section, we attempt to at least qualify how rare the compact, red-looking, star-forming galaxies are. Both stellar population evolution and dynamical evolution of any compact young stellar system will lead to an expansion in size and dimming in brightness. The observation of compact and old non-star-forming objects means that once they were much more compact and brighter while they were young – if they formed in isolation. There exist the compact star-forming galaxies, so-called Blue Compact Dwarf galaxies (BCDs), some of them are as compact as cE, but they are less luminous than cEs. Note that all BCDs are not, in general, compact galaxies. In most cases, they are BCDs due to presence of blue compact star-forming region on the top of underlying extended relatively old component. The brightest BCD in the Virgo cluster, VCC 324, has a total luminosity of $M_r = -17.46$ mag and overall effective radius of 0.96 kpc. Selecting compact BCDs of sizes similar to cEs from Meyer et al. (2014) sample we find a clear offset in magnitude distribution where cEs are on average a magnitude brighter than compact BCDs.

To get a more statistically complete view of compact galaxies like SDSS J1229+0001 we visually analyse morphology and $g - i$ colour index of a sample selected from SDSS. We select the galaxies sample from the SDSS catalogue within the redshift range $z < 0.02^{10}$ which have effective radii (in the SDSS catalogue it is Petrosian half-light radius) $< 0.6 \text{ kpc}^{11}$.

¹⁰ We have chosen this redshift range because beyond 0.02 the morphological classification may not be reliable and also beyond this with a typical SDSS PSF of $1''$ it is not sufficient to measure the R_e of these compact galaxies.

¹¹ There are ~ 500 galaxies and a significant majority of them are BCD type.



Figure 9. The SDSS colour image of SDSS J112308.77+624845.6 with a field of view $1' \times 1'$.

We find only one additional example, SDSS J112308.77+624845.6 a very similar morphology galaxy, see Figure 9. Which have a Petrosian half light radius, measured by the SDSS, of 534 pc. The $g - i$ colour, before correcting the internal extinction, index is 1.3 mag and emission line metallicity, $12 + \log(\text{O}/\text{H})$, is 8.54. We find that the $g - i$ colour index larger than 1.3 mag is an extreme for similar mass galaxies and interestingly non of Virgo cluster galaxies, of both star-forming or non star-forming types, have that $g - i$ colour index.

4.3 Star-Formation and Evolution

The detection of star-formation activity in early-type galaxies is not new, nor is the presence of significant amount of neutral Hydrogen (HI). A dedicated study of HI distribution in Es by ATLAS-3D team detected HI in 40 percent of Es outside a cluster environment (Serra et al. 2012). Recent data release of HI survey by ALPHA-APHA team reported that SDSS J1229+0001 has total HI mass of $4 \times 10^8 M_\odot$ and corresponding value of $\text{Log}[M(\text{HI})/M_\star]$ is -0.62. Presence of cold gas in Es has been interpreted as indicating a continuing growth of these galaxies up to the recent past (Serra & Oosterloo 2010; Thom et al. 2012). They may accrete cold gas directly from the field or via merger (major/minor). Although SDSS J1229+0001 has the gas mass $4 \times 10^8 M_\odot$ and gas mass fraction -0.62 the observed star-formation rate of $0.26 M_\odot/\text{yr}$ seems to an upper limit for similar mass ($M_B \approx -16.5$ mag) star-forming dwarf galaxies (Lee et al. 2009, Figure 6). Assuming an HI consumption fraction of 10%, the star-formation activity only last 160 Myr with current SFR. So it is very likely to be just a temporary phase.

Hallenbeck et al. (2012) in a study of a sample of gas bearing early-type dwarf galaxies in Virgo cluster propose two possibilities – either such galaxies have recently accreted their gas or they are in the last stages of star-formation.

In particular, for those which have detectable star-forming activity they suggest the later. Is the similar case for the SDSS J1229+0001? The observed relatively high emission line metallicity may be well explained according to the fundamental relation between gas-mass fraction star-formation rate and emission line metallicity where where emission line metallicity anti-correlates with gas-mass fraction for given star-formation rate (Lara-López et al. 2010). We also find that two of Hallenbeck et al. (2012) objects, only for which we can derive emission line metallicity from the SDSS spectroscopy, have similar value of $12 + \log(\text{O}/\text{H}) = \sim 8.45$. The study of Geha et al. (2012) showed that field galaxies of dwarf regime always have some residual star formation. The SDSS J1229+0001 is located in relatively far from the massive halo, so the presence of star-formation is in line of Geha et al prediction.

How would it evolve after cease to form star in the centre? Any dynamical and stellar population evolution of compact star-forming object is likely to decrease the surface brightness and expand the size (Assmann et al. 2013; Pfalzner & Kaczmarek 2013; Wellons et al. 2015; El-Badry et al. 2016). It is certain that the central surface brightness in optical band decreases as it becomes older. Does it look similar to a typical low-surface brightness galaxy dE/dS0 or still remain low mass high surface brightness early-type galaxy like E/S0? The mean surface brightness $17.53 \text{ mag arcsec}^{-2}$ in H-band is ~ 2 mag higher compared to average value of dE studied in Janz et al. (2014). Similarly, it is unusually compact having H-band half-light radius similar to NGC4486A. NGC4486A is a compact low mass-early type galaxy in Virgo cluster which also shows unusual burst of star-formation at the centre (Prugniel et al. 2011). NGC4486A is >4.5 mag brighter than SDSS J1229+0001. In this regard, SDSS J1229+0001 maybe considered a low luminosity version of NGC4486A.

In summary, we find a couple of ignored morphology galaxy which maybe more similar to high z galaxies (e.g. Tadaki et al. 2015). The red colour and relatively high emission line metallicity of these objects might suggest a deficiency gas mass fraction while actively forming stars at the end stage of evolution. Compact star-burst and dust-dominated galaxies are expected to be common in the early universe – are these galaxies a low redshift counterpart? In fact, the formation of compact ellipticals in the high-redshift universe has been associated with merger-induced star-burst activity with dissipative collapse of star-forming gases (Kormendy & Sanders 1992; Hopkins et al. 2009). It is also important explore why there are no such compact, massive, galaxies (of both star-forming and non star-forming types) in the nearby universe. While more detailed comparative analysis of structural and stellar population properties of more complete sample would be necessary to establish an unambiguous evolutionary connection, these observational findings themselves maybe an important step toward toward this. In the next series of publication we aim to explore further.

ACKNOWLEDGMENTS

This study has made use of NASA’s Astrophysics Data System Bibliographic Services and the NASA/IPAC Extra-

galactic Database (NED). SDSS data were queried from the SDSS archive. Funding for the SDSS/SDSS-III has been provided by the Alfred P. Sloan Foundation, the Participating Institutions, the National Science Foundation, the U.S. Department of Energy, the National Aeronautics and Space Administration, the Japanese Monbukagakusho, the Max Planck Society, and the Higher Education Funding Council for England. The SDSS Web Site is <http://www.sdss.org>.

REFERENCES

- Abazajian, K. N., Adelman-McCarthy, J. K., Agüeros, M. A., et al. 2009, *ApJS*, 182, 543
- Amblard, A., Riguccini, L., Temi, P., et al. 2014, *ApJ*, 783, 135
- Assmann, P., Fellhauer, M., Wilkinson, M. I., Smith, R., & Blaña, M. 2013, *MNRAS*, 435, 2391
- Baldwin, J. A., Phillips, M. M., & Terlevich, R. 1981, *PASP*, 93, 5
- Bekki, K., Couch, W. J., Drinkwater, M. J., & Gregg, M. D. 2001, *ApJ*, 557, L39
- Bruzual, G. & Charlot, S. 2003, *MNRAS*, 344, 1000
- Calzetti, D., Armus, L., Bohlin, R. C., et al. 2000, *ApJ*, 533, 682
- Charlot, S. & Fall, S. M. 2000, *ApJ*, 539, 718
- Chen, C.-W., Côté, P., West, A. A., Peng, E. W., & Ferrarese, L. 2010, *ApJS*, 191, 1
- Chilingarian, I., Cayatte, V., Revaz, Y., et al. 2009, *Science*, 326, 1379
- Chilingarian, I. & Zolotukhin, I. 2015, *Science*, 348, 418
- Chilingarian, I. V. & Bergond, G. 2010, *MNRAS*, 405, L11
- Chilingarian, I. V. & Mamon, G. A. 2008, *MNRAS*, 385, L83
- Choi, P. I., Guhathakurta, P., & Johnston, K. V. 2002, *AJ*, 124, 310
- Colless, M., Dalton, G., Maddox, S., et al. 2001, *MNRAS*, 328, 1039
- da Cunha, E., Charlot, S., & Elbaz, D. 2008, *MNRAS*, 388, 1595
- Denicoló, G., Terlevich, R., & Terlevich, E. 2002, *MNRAS*, 330, 69
- di Serego Alighieri, S., Bianchi, S., Pappalardo, C., et al. 2013, *A&A*, 552, A8
- Doyle, M. T., Drinkwater, M. J., Rohde, D. J., et al. 2005, *MNRAS*, 361, 34
- El-Badry, K., Wetzell, A., Geha, M., et al. 2016, *ApJ*, 820, 131
- Geha, M., Blanton, M. R., Yan, R., & Tinker, J. L. 2012, *ApJ*, 757, 85
- Graham, A. W., Dullo, B. T., & Savorgnan, G. A. D. 2015, *ApJ*, 804, 32
- Graham, A. W. & Guzmán, R. 2003, *AJ*, 125, 2936
- Hallenbeck, G., Papastergis, E., Huang, S., et al. 2012, *AJ*, 144, 87
- Hopkins, A. M., Schulte-Ladbeck, R. E., & Drozdovsky, I. O. 2002, *AJ*, 124, 862
- Hopkins, P. F., Bundy, K., Murray, N., et al. 2009, *MNRAS*, 398, 898
- Huxor, A. P., Phillipps, S., & Price, J. 2013, *MNRAS*, 430, 1956
- Huxor, A. P., Phillipps, S., Price, J., & Harniman, R. 2011, *MNRAS*, 414, 3557
- Janz, J., Laurikainen, E., Lisker, T., et al. 2014, *ApJ*, 786, 105
- Janz, J. & Lisker, T. 2008, *ApJ*, 689, L25
- Kennicutt, Jr., R. C. 1998, *ARA&A*, 36, 189
- Kormendy, J. 1985, *ApJ*, 295, 73
- Kormendy, J., Fisher, D. B., Cornell, M. E., & Bender, R. 2009, *ApJS*, 182, 216
- Kormendy, J. & Sanders, D. B. 1992, *ApJ*, 390, L53
- Lara-López, M. A., Cepa, J., Bongiovanni, A., et al. 2010, *A&A*, 521, L53
- Lee, J. C., Kennicutt, Jr., R. C., Funes, S. J. J. G., Sakai, S., & Akiyama, S. 2009, *ApJ*, 692, 1305
- Lisker, T., Grebel, E. K., Binggeli, B., & Glatt, K. 2007, *ApJ*, 660, 1186
- Makarov, D. & Karachentsev, I. 2011, *MNRAS*, 412, 2498
- Marino, R. A., Rosales-Ortega, F. F., Sánchez, S. F., et al. 2013, *A&A*, 559, A114
- Meyer, H. T., Lisker, T., Janz, J., & Papaderos, P. 2014, *A&A*, 562, A49
- Mieske, S., Infante, L., Hilker, M., et al. 2005, *A&A*, 430, L25
- Misgeld, I. & Hilker, M. 2011, *MNRAS*, 414, 3699
- Murphy, E. J., Condon, J. J., Schinnerer, E., et al. 2011, *ApJ*, 737, 67
- Norris, M. A., Kannappan, S. J., Forbes, D. A., et al. 2014, *MNRAS*, 443, 1151
- Osterbrock, D. E. 1989, *Astrophysics of gaseous nebulae and active galactic nuclei*
- Paudel, S., Hilker, M., Ree, C. H., & Kim, M. 2016, *ApJ*, 820, L19
- Paudel, S., Lisker, T., Hansson, K. S. A., & Huxor, A. P. 2014, *MNRAS*, 443, 446
- Paudel, S., Lisker, T., Kuntschner, H., Grebel, E. K., & Glatt, K. 2010, *MNRAS*, 405, 800
- Pfalzner, S. & Kaczmarek, T. 2013, *A&A*, 559, A38
- Price, J., Phillipps, S., Huxor, A., et al. 2009, *MNRAS*, 397, 1816
- Prugniel, P., Zeilinger, W., Koleva, M., & de Rijcke, S. 2011, *A&A*, 528, A128
- Rieke, G. H., Alonso-Herrero, A., Weiner, B. J., et al. 2009, *ApJ*, 692, 556
- Ryden, B. S., Terndrup, D. M., Pogge, R. W., & Lauer, T. R. 1999, *ApJ*, 517, 650
- Sandage, A. & Binggeli, B. 1984, *AJ*, 89, 919
- Serra, P., Oosterloo, T., Morganti, R., et al. 2012, *MNRAS*, 422, 1835
- Serra, P. & Oosterloo, T. A. 2010, *MNRAS*, 401, L29
- Stringer, M., Trujillo, I., Dalla Vecchia, C., & Martinez-Valpuesta, I. 2015, *MNRAS*, 449, 2396
- Tadaki, K.-i., Kohno, K., Kodama, T., et al. 2015, *ApJ*, 811, L3
- Thom, C., Tumlinson, J., Werk, J. K., et al. 2012, *ApJ*, 758, L41
- Trujillo, I., Cenarro, A. J., de Lorenzo-Cáceres, A., et al. 2009, *ApJ*, 692, L118
- Trujillo, I., Conselice, C. J., Bundy, K., et al. 2007, *MNRAS*, 382, 109
- Wellons, S., Torrey, P., Ma, C.-P., et al. 2015, *MNRAS*, 449, 361